Numerical Analysis of Cyclic Loading and Fatigue Behavior of Alkali-Activated Concrete Beams

Ashish Anand[1], *Imran* Kuttagola[2*], and *M H* Prashanth[1]

[1]Department of Civil Engineering, National Institute of Technology Karnataka, Surathkal, Mangalore 575025, India
[2]Assistant Professor, Department of Civil Engineering, Madanapalle Institute of Technology & Science (MITS), Deemed to be University, Madanapalle, Andhra Pradesh, India-517325

Abstract. Alkali-activated concretes (AAC) are emerging as sustainable alternatives to Portland cement concrete (PCC) due to their substantially lower carbon emissions; however, their fatigue behaviour requires further investigation. This study numerically evaluates the monotonic and fatigue performance of fly ash-based AAC in comparison with PCC of comparable strength. Three-point bending under monotonic loading is first simulated using ABAQUS/CAE. A two-dimensional notched beam specimen of size 262.5 mm × 75 mm with a centrally located bottom notch of 15 mm × 3 mm is modelled. Two strength grades of AAC and corresponding PCC mixes are analysed. Ultimate load, mid-span deflection, and crack mouth opening displacement are obtained from history outputs. The monotonic response is then used to define constant-amplitude cyclic loading for fatigue analysis, with load ranges of 20-80% and 25-95% of the ultimate load. Structural responses under cyclic loading are examined and compared. Since finite element modelling cannot directly capture the complete fatigue life of quasi-brittle materials, fatigue resistance is approximated using the number of cycles associated with the initial rapid deformation stage, assumed to represent 10% of the total fatigue life. From the observed results, AAC performed higher fatigue strength with respect to the PCC, highlighting its potential for sustainable constructions.

1 Introduction

Growing concerns related to global warming and climate change have driven a significant shift across engineering disciplines toward the adoption of environmentally sustainable materials and construction practices. Ordinary Portland cement (OPC) production is associated with high energy consumption and substantial CO_2 emissions, which has motivated the development of alternative binders with reduced environmental impact. One of the most promising developments is alkali-activated binders, which are the best alternatives for OPC binders. Alkali-activated binders are the strongest precursors that

* Corresponding author: imranswathi2020@gmail.com

achieve denser matrices in the concrete by adding alkaline solutions to the silica and alumina-rich material sources [1].

The concrete is a heterogeneous quasi-brittle material with pores and microcracks that generate the weakest phase in the matrix before the application of external load [2]. These weak phases under the application of cyclic loading act as stress concentration zones that progress to the damage initiation, and gradually microcracks propagate into the macrocracks. This will reduce the effective cross-section and lead to fatigue failure [3]. Also, modern design methods involve lighter and slender structures, susceptible to higher stress concentrations and more oscillating loads, which highlights the requirement for advanced fatigue analysis.

The durability and related service life analysis is critically dependent on the fatigue behaviour of concrete, which has attracted several researchers over the past decades. Taliercio et al. (1996) investigated the mechanical properties of cylindrical specimens under cyclic triaxial loading and reported that the interactions between axial and confining stress greatly affects its fagigue life under stresses in phase opposition. In contrast, an increase in the mean lateral confining pressure was found to enhance fatigue performance by delaying damage accumulation and crack propagation. And also, fatigue life improved with an increase in mean lateral confinement [4]. Arthur et al. (2015) reported that the plain concrete and fibre reinforced specimens under lower frequencies exhibited lower fatigue life as compared to those tested under higher frequencies [5]. Stanislav et al. (2015) conducted a comparative investigation of OPC and geopolymer concrete. The geopolymer concrete showed lower tensile strengths due to its brittle nature, but showed higher fatigue lives [6]. Further, Zhang et al. (2021) used an energy-dissipation approach for fatigue analysis of plain concrete at different stresses and found that higher stress levels yield higher fatigue damage [7].

Knowing the fatigue life of concrete is of utmost importance for long term durability of structures. A sufficient amount of work has been carried out in assessing the fracture as well as fatigue behavior of OPC binder concrete. Since AAC is the way ahead for its numerous advantages, its characteristics need to be studied as well. In the last decade, a good amount of research has been done, which shows its physical and chemical properties, etc. But there is a gap in research regarding its long-term durability against fatigue load in structures. Therefore, the present study's novelty lies in systematically investigating the fatigue behaviour of alkali-activated concrete under different constant-amplitude load cycles and elucidating its distinguishing fatigue characteristics in comparison with conventional OPC concrete.

2 Numerical Framework and Model Description

Numerical simulations for both monotonic and cyclic loading were performed in the ABAQUS software. To ensure controlled crack initiation and propagation at the mid-span, a notch was introduced at the bottom centre of the beam. The beam geometry includes a notch depth of 15 mm with a notch width of 3 mm. Monotonic loads were applied centrally downward point load, and the response obtained from these static analyses was subsequently used to define the load ranges for the fatigue simulations.

Fatigue analyses were conducted using constant-amplitude cyclic loading derived as a percentage of the ultimate load of monotonic tests. Four different concrete types were considered in the study: fly ash blended alkali-activated concrete cured at 22 °C (FC22) and 50 °C (FC50), along with corresponding plain cement concrete mixes (PCC22 and PCC50) designed to achieve similar ultimate compressive strengths as their AAC counterparts. The concrete damaged plasticity model was used to simulate the nonlinear response of concrete under both monotonic and fatigue loading. Material parameters for the CDP model were

selected based on reported literature and recommendations from the ABAQUS Theory Manual [8], and the adopted values for all concrete mixes are summarized in Table 1. To enhance numerical stability and convergence, a viscosity parameter of 5×10^{-4} Ns/mm² was introduced following a parametric investigation, consistent with previous studies [9].

The uniaxial compressive and tensile stress–strain relationships, along with Poisson's ratio for alkali-activated concrete, were defined based on experimental data reported by Robert et al. [1]. For plain cement concrete, the corresponding stress–strain behaviour was modelled using the constitutive relationships proposed by Popovics [10]. In the fatigue simulations, stiffness degradation associated with tensile cracking was modelled with zero compression recovery, whereas compressive crushing damage was assigned a 0.8 tension factor to realistically represent cyclic damage evolution.

Table 1. Input parameters of ABAQUS.

Parameters	FC-22	FC-50	PCC-22	PCC-50
Density [kg/m³]	2390	2390	2390	2390
Elastic modulus [MPa]	12902.60	33462.16	16501.18	21754.40
The Poisson ratio	0.126	0.128	0.184	0.185
The Angle of Dilation	37	37	37	37
The Eccentricity	0.11	0.11	0.11	0.11
f_{b0}/f_{c0}	1.159	1.159	1.159	1.159
K value	0.6666	0.6666	0.6666	0.6666
The Viscous factor [Ns/mm²]	0.0005	0.0005	0.0005	0.0005

3 Modelling and Analysis

A numerical investigation of the bending behaviour of three-point bending specimens was carried out using the commercial finite element software ABAQUS. The concrete beam was modelled as a two-dimensional deformable body using a shell-based planar representation, with its geometry defined according to the specified dimensions. The loading and support components were modelled as two-dimensional discrete rigid bodies using wire-based features to realistically represent the load applicator and supports.

The material properties of concrete were first defined, and to capture the nonlinear response of concrete, particularly cracking in tension and crushing in compression, the concrete damaged plasticity (CDP) model available in ABAQUS was employed. The CDP formulation inherently accounts for tension-compression asymmetry by allowing the definition of independent uniaxial tensile and compressive stress-strain relationships along with separate damage evolution laws. The suitable sections were generated and assigned to the sections of beams under plane stress conditions with 100 mm thickness. An assembly model was adopted to facilitate the interactions and mesh creation. A cut-geometry tool is used to create a sharp notch for proper crack initiation. A surface-surface contact interactions were adopted to define the interactions between the beam section, supports and loading conditions. The different supports and loading conditions were assigned using master surface options, and the beam geometry was assigned using the slave surface option. A downward displacement of 0.5 mm is applied on the load cell at the centre of the beam for static analysis

under displacement-controlled condition, whereas the load-controlled conditions were applied for the fatigue analysis.

CPS4R quadrilateral elements were used for beam discretisation under plane stress conditions. A refined mesh of 2 mm was employed in the vicinity of contact regions to minimize numerical issues such as overclosure. The analysis results were stored in the ABAQUS output database (.odb) file, and post-processing was carried out using the Visualization module to examine deformed configurations, contour and vector plots, animations, and X–Y response curves.

4 Results and Interpretation

4.1 Static Loading Behaviour

The resulting load–displacement and load-CMOD relationships from the displacement-controlled three-point test analyses were obtained from the numerical simulations and are presented for comparison. Key response parameters are tabulated in Table 2.

Table 2. Maximum Load and Displacement at failure.

Parameters	FC-22	FC-50	PCC-22	PCC-50
Maximum load at failure(N)	3180.59	4987.24	2040.44	3460.12
Max displacement at failure (mm)	0.076356	0.043736	0.036832	0.046559
Max CMOD at failure (mm)	0.014713	0.006105	0.004825	0.005917

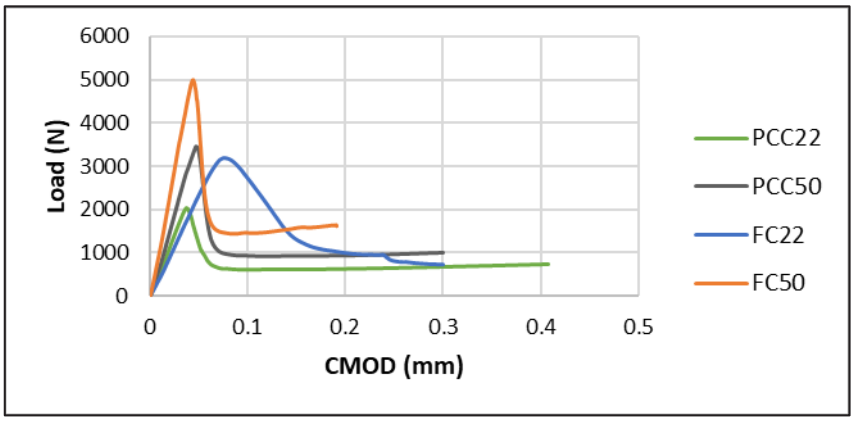

Fig. 1. Load-CMOD plots for different specimens.

The load-CMOD relationships are compared in Fig. 1. The peak load for FC beams and particularly the FC-50 beam is significantly higher than the corresponding similar strength PCC beams due to high strength characteristics of Alkali activated binders and due to curing at elevated temperatures. Also, the peak deflection and CMOD at peak load is lowest for FC22 due to the lowest elastic modulus out of all.

4.2 Fatigue Loading Behaviour

Cyclic loading tests were performed using a load range corresponding to 20-80% of the previously determined maximum static failure load. The specific load limits adopted for each specimen are summarized in Table 3. Initially, a single loading cycle within the 20-80% load range was applied at a frequency of 1 Hz to establish the cyclic response under controlled conditions. The structural responses were then compared with those of the static FEA test. Comparing the upper and lower load limit attained (Table 4) during one cycle of loading and unloading, to that of the result of static tests, it is seen that both upper and lower load limit obtained during one load cycle of fatigue test are slightly lower than the corresponding 20% and 80% of peak load in the static test.

Table 3. Load values for 20%-80% range.

	FC22		**FC50**		**PCC22**		**PCC50**	
	20%	80%	20%	80%	20%	80%	20%	80%
Load (N)	640	2570	1000	3990	400	1630	700	2770

Table 4. Loading and unloading cycle values.

	FC22		**FC50**		**PCC22**		**PCC50**	
	Lower	Upper	Lower	Upper	Lower	Upper	Lower	Upper
Static test	640	2570	1000	3990	400	1630	700	2770
Loading and unloading Cycle	627	2551	980	3966	394	1629	676	2753

Subsequently, twenty fatigue load cycles were applied within the same 20-80% load range at 1 Hz. The variation of mid-span deflection with the number of cycles for all specimens is shown in Fig. 2. A rapid increase in deflection and CMOD is observed during the initial 4-7 cycles, followed by a stabilized phase where the response parameters increase at a much slower rate. Beyond the seventh cycle, no significant change in deflection or CMOD is noted up to the twentieth cycle, indicating a stable damage accumulation phase. Similar three-stage fatigue behaviour has been reported for concrete and quasi-brittle materials in the literature. In the present study, the commonly adopted 10%-80%-10% distribution is used only as a qualitative interpretative framework to describe the relative dominance of each stage, rather than as a definitive quantification of fatigue life. Since full fatigue-life (S-N) characterization was not within the scope of this numerical investigation, this assumption is acknowledged as a limitation of the study.

It is noted that the concrete damaged plasticity (CDP) model employed in this study does not incorporate an explicit cumulative fatigue damage formulation. Instead, fatigue effects are indirectly captured through progressive stiffness degradation and damage evolution under cyclic loading. Consequently, the numerical results presented herein should be interpreted as comparative indicators of fatigue resistance and damage tolerance among the investigated concrete grades, rather than as absolute fatigue life predictions. The objective of the present numerical study is therefore to highlight relative fatigue performance trends between alkali-activated concrete and conventional cement concrete under identical loading conditions.

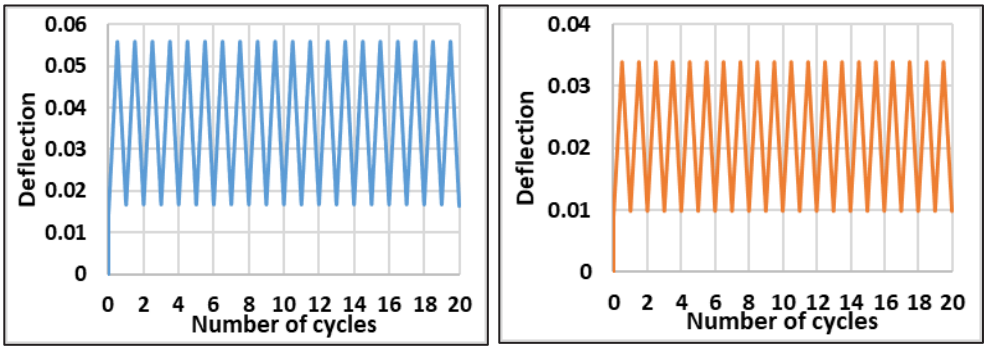

Fig. 2. The Deflection vs Number of cycles for twenty load cycles.

4.3 High-Amplitude Fatigue Loading Response

To accelerate failure and examine crack growth under severe cyclic conditions, a higher-amplitude fatigue load ranging from 25% to 95% of the peak static load was applied at a frequency of 1 Hz. The corresponding load limits are summarised in Table 5.

The variation of maximum CMOD with the number of cycles under high-amplitude loading is presented in Fig. 3. The CMOD evolution clearly demonstrates rapid crack opening and damage accumulation. For PCC22 and FC50 specimens, failure initiates within the first loading cycle, indicating highly unstable crack propagation under severe cyclic stress levels. The FC22 specimen fails during the loading phase of the second cycle, whereas PCC50 sustains up to three cycles before failure, with crack instability initiating during the unloading phase of the third cycle.

Table 5. Load values for 25%-95% range.

	FC22		FC50		PCC22		PCC50	
	25%	95%	25%	95%	25%	95%	25%	95%
Load (N)	800	3040	1250	4730	510	1930	870	3280

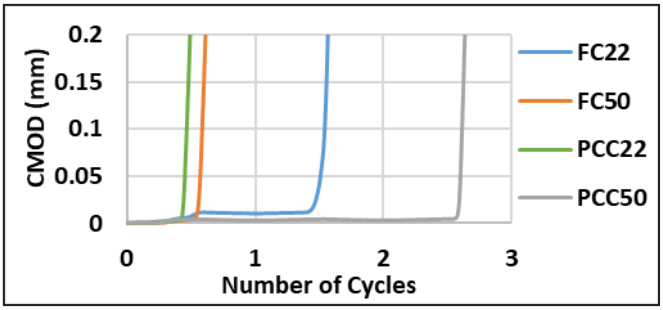

Fig. 3. Maximum CMOD vs Number of Cycles.

4.4 Crack Initiation and Damage Evolution

The crack initiation and propagation behaviour under both monotonic and cyclic loading can be effectively interpreted from global response indicators such as load–deflection curves, CMOD evolution, hysteresis behaviour, and cycle-wise stiffness degradation. Under monotonic loading, crack initiation is identified by the deviation from linearity in the load–deflection response, accompanied by a sharp increase in CMOD, indicating tensile cracking

at the notch tip. A steady crack propagation is observed after peak due to tensile damage in the matrix. The hysteresis loops appeared during initial loadings and reflect the progressive damage. A fast growth of cracks corresponds to the initiation of crack and with progressive growth of crack, a stable response is achieved. A fast increase in CMOD at larger load ranges shows an unstable and premature failure.

4.5 Influence of Strength Grade on Fatigue Performance

The effect of the grade of concrete on the fatigue behaviour of both alkali-activated and plain concrete is studied for the specimens cured at 22°C and 50°C under similar loading conditions. When a static load is applied, FC-50 and PCC-50 specimens demonstrated higher peak loads and smaller displacements. Whereas cyclic loads FC-50 demonstrated an early failure at 25-95% range, despite performing well at static loads. This shows that the Alkali-Activated concretes show brittle behavious inspte of high strengths. In contrary, FC-22 performs well resisting more cycles despite lower strengths. The strength of the concrete plays a crucial role in deciding the fatigue performance under both static loads and dynamic loads, especially in alkali-activated concretes. Hence, fatigue analysis is crucial along with static analysis for deciding the Alkali-activated grades in constructions which undergoes reugular cyclic loading conditions.

5 Conclusion

The numerical results under static and fatigue analysis have been used to draw the following conclusion:

1) Specimens with higher strength (FC50 and PCC50) exhibited greater ultimate load capacity under monotonic loading than their lower-grade counterparts (FC22 and PCC22). Whereas the alkali-activated specimens showed a higher peak load compared to the plain concrete specimens, highlighting its importance.
2) Specimens with lower strengths (FC-22) demonstrated larger deflections at failure due to lower modulus of elasticity, whereas alkali-activated specimens demonstrated brittle behaviour with steeper plots after peak load.
3) Under the lower-amplitude load cycles (20-80% of the ultimate static load), the FE model showed negligible changes in CMOD or mid-span deflection after a few initial cycles, indicating that the material model was unable to capture the subtle damage accumulation occurring during the stable secondary stage of fatigue.
4) When subjected to higher-amplitude fatigue loading (25-95% of the ultimate static load), all beam specimens failed within three loading cycles, with FC50 and PCC22 failing during the first cycle.
5) When beams were applied with the higher load cycles (25-95%), all specimens failed within 3 cycles of loading and unloading, with FC50 and PCC22 failing within one cycle.

References

1. R. Thomas, J.S. Peethamparan, Alkali-activated concrete: Engineering properties and stress–strain behavior. Constr. Build. Mater. **93**, 49–56 (2015). https://doi.org/10.1016/j.conbuildmat.2015.04.039
2. A. Hillerborg, M. Modeer, P. Petersson, Analysis of crack formation and crack growth in concrete by means of fracture mechanics and finite elements. Cem. Concr. Res. **6**, 773–782 (1976). https://doi.org/10.1016/0008-8846(76)90007-7

3. T.C.C. Hsu, Fatigue of plain concrete. ACI J. **78**, 292–305 (1981). https://doi.org/10.14359/6927
4. A.L.F. Taliercio, E. Gobbit, Experimental investigation on the triaxial fatigue behavior of plain concrete. Mag. Concr. Res. **48 (176)**, 157–172 (1996). https://doi.org/10.1680/macr.1996.48.176.157
5. A. Medeiros, X. Zhang, G. Ruiz, R. Yu, M. de Souza Lima Velasco, Effect of the loading frequency on the compressive fatigue behavior of plain and fiber reinforced concrete. Int. J. Fatigue **70**, 342–350 (2015). https://doi.org/10.1016/j.ijfatigue.2014.08.005
6. S. Stanislav, V. Bílek, Z. Keršner, Comparison of fatigue parameters of alkali-activated and ordinary Portland cement-based concretes. Int. J. Res. Eng. Technol. 2319-1163 (2015). https://doi.org/10.15623/ijret.2014.0325032
7. Q. Zhang, L. Wang, Investigation of stress level on fatigue performance of plain concrete based on energy dissipation method. Constr. Build. Mater. **269**, 121287 (2021). https://doi.org/10.1016/j.conbuildmat.2020.121287
8. Abaqus Theory Manual, Version 6.12, Dassault Systèmes, (2012)
9. P. Kmiecik, M. Kaminski, Modelling of reinforced concrete structures and composite structures with concrete strength degradation taken into consideration. Arch. Civ. Mech. Eng. **11 (3)**, 623–636 (2011). https://doi.org/10.1016/S1644-9665(12)60105-8
10. S. Popovics, A numerical approach to the complete stress–strain curve of concrete. Cem. Concr. Res. **3**, 583–599 (1973). https://doi.org/10.1016/0008-8846(73)90096-3
11. N.K. Banjara, K. Ramanjaneyulu, S. Sasmal, V. Srinivas, Flexural fatigue performance of plain and fibre reinforced concrete. Trans. Indian Inst. Met. **69 (2)**, 373–377 (2016). https://doi.org/10.1007/s12666-015-0770-y